LEGENDS TO SUPPLEMENTARY INFORMATION

Supplementary Figure 1. IHC and proliferation analysis of *pten*-deficient mammary tumors

A. Induced expression of estrogen receptor α (ERα) in AME vs PDA tumors. Student's t test, p=0.0005, n≥3.
B. Induced expression of Ki67 in PDAs vs AMEs. Student's t test, p=0.0031, n≥3.
C. Enlarged immunohistochemistry images of AMEs and PDAs shown in Figure 1I. N=6.
D. In vitro growth curves of independent AME tumor cell lines incubated with indicated concentrations of β-estradiol. Student's t test, *p<0.05, **p<0.01; ***p<0.001, n=2.

Supplementary Figure 2. Proliferation and apoptosis analyses of AME and PDA cells following orthotopic transplantation into NOD/SCID mice

Shown are representative IHC images of phospho-H3, Ki67 and activated caspase 3 of mammary glands injected with AME or PDA cells at indicated time points. n≥3.

Supplementary Figure 3. GSEA reveals distinct pathways in PDAs versus AMEs

Complete GSEA of AMEs (blue) versus PDAs (red) using canonical pathways (c2.all, v4.0, Broad Institute) visualized using Cytoscape Enrichment Map. Green lines connect overlapping pathways. Size of the circles corresponds with levels of enrichment (normalized enrichment score) whereas thickness of lines corresponds with degree of overlap. p<0.001, FDR<0.001. PDA n=8, AME n=13.

Supplementary Figure 4. g:Profiler analysis of AMEs versus PDAs. p<0.05. PDA n=8, AME n=13.

Supplementary Figure 5. aCGH analysis showing distinct genetic alterations in PDAs versus AMEs

Shown is a list of genes with significant copy number changes in PDAs versus AMEs including chromosomal location and frequency of alterations. PDA n=5, AME n=5.

Supplementary Figure 6. Schematic representation of *Cul9* (a) and *Cbl* (b), and relative location (asterisks) of mutations identified in PDAs. PDA n=7, AME n=3.

Supplementary Figure 7. Kaplan-Meier survival analysis for patients with miR-145-low/PTEN-low expression showing a trend toward significantly worse DFS compared to patients with miR-145-high/PTEN-low expression.

Supplementary Figure 8. miR-143/145 knockdown cooperates with *pten* loss by activating the Ras pathway

A. In vitro growth curves of independent AME tumor cell lines transduced with miR-143/145 decoy. n≥5.
B. Epithelial marker analysis of AME and PDA tumors for ERα, K18 and K14. n≥3.
C. Representative Western Blot analysis of PTEN knockdown by lentiviral shRNA. n≥3.
D. In vitro growth curves of HC11 cells transduced with miR-143/145 decoy, *pten* shRNA or both. n≥3.
E. Western blot quantification showing elevated phospho-Erk levels in HC11 cells treated with both miR-143/145 decoy and *pten* shRNA compared to cells transduced with only miR-143/145 decoy, or only *pten* shRNA. n≥8.

F. Quantitative RT-PCR analysis of indicated predicted miR-143/145 targets following miR-143/145 overexpression. n=3.

Supplementary Figure 9. Distinct levels of activation of 18 signaling pathways in AMEs vs PDAs

* denotes significant differences. Red – induction in PDAs; green – induction in AMEs. PDA n=8, AME n=13.

Figure S1

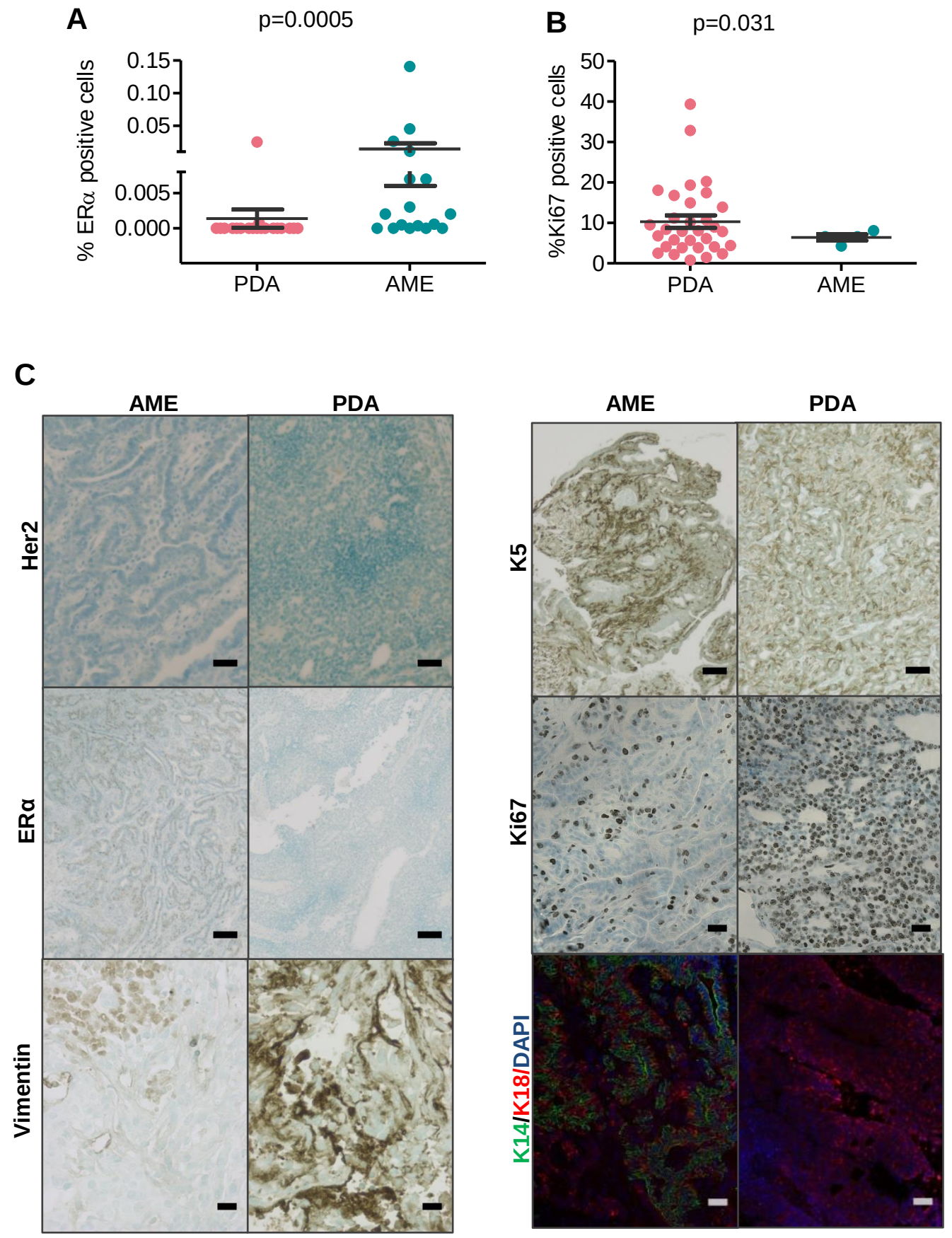
A
p=0.0005
% ERα positive cells
0.15
0.10
0.05
0.005
0.000
PDA
AME
B
p=0.031
%Ki67 positive cells
50
40
30
20
10
0
PDA
AME
C
AME
PDA
Her2
ERα
Vimentin
AME
PDA
K5
Ki67
K14/K18/DAPI

D

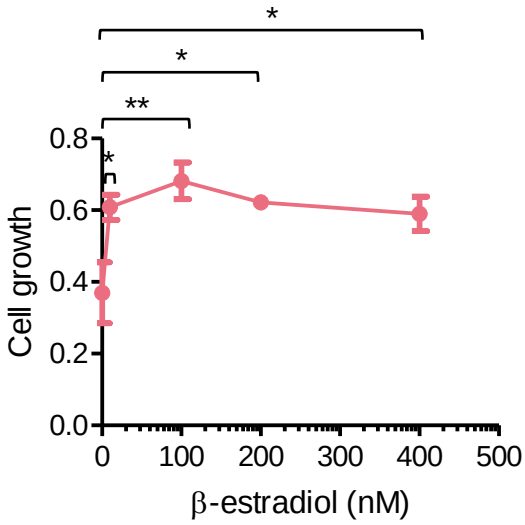
*
*
**
*
Cell growth
0.0
0.2
0.4
0.6
0.8
0
100
200
300
400
500
β-estradiol (nM)

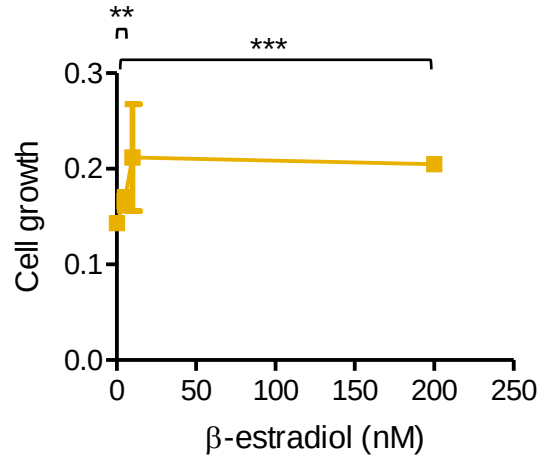
**
***
Cell growth
0.0
0.1
0.2
0.3
0
50
100
150
200
250
β-estradiol (nM)

Figure S2

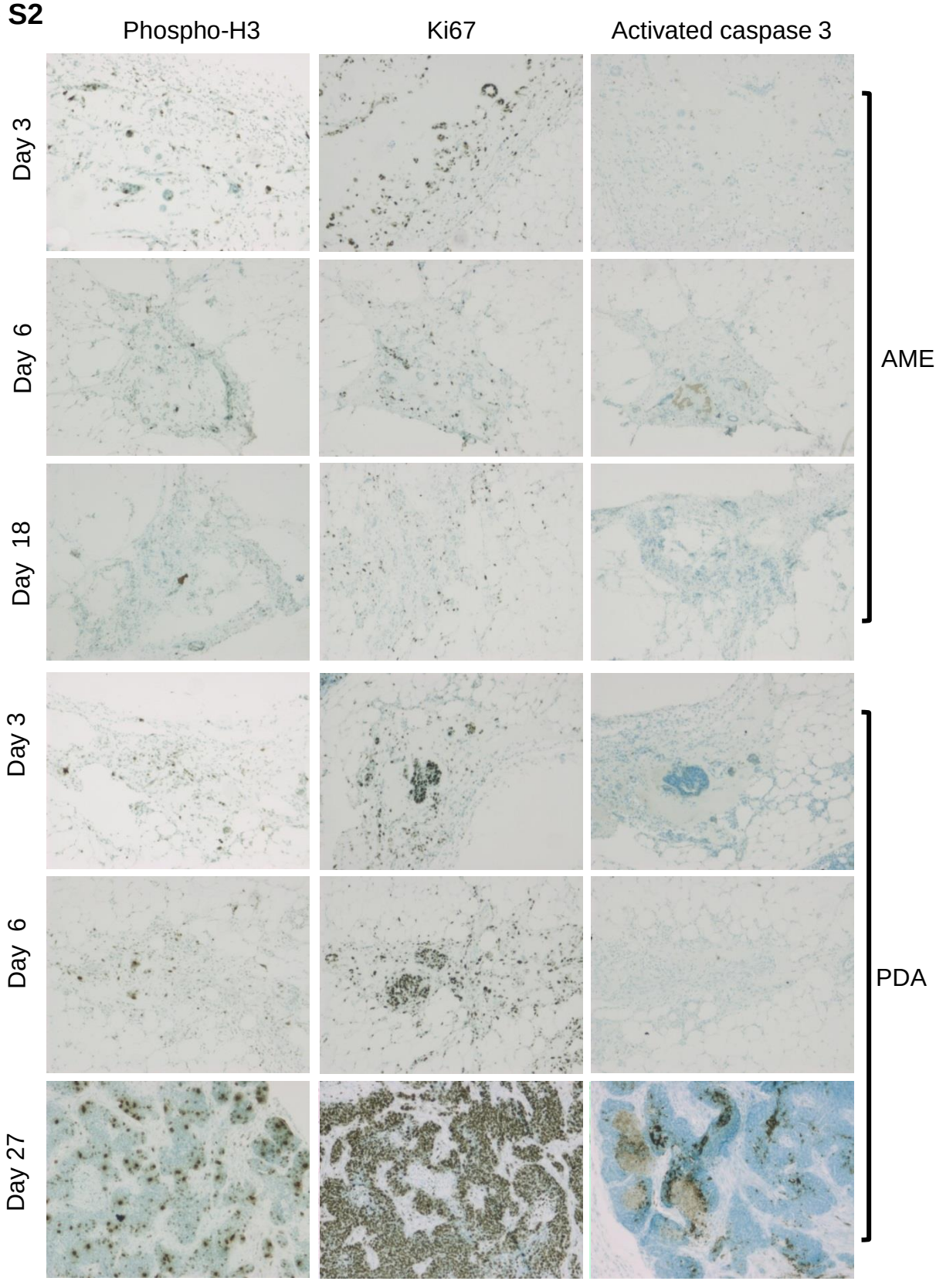
Phospho-H3
Ki67
Activated caspase 3
Day 3
Day 6
Day 18
AME
Day 3
Day 6
Day 27
PDA

Figure S3

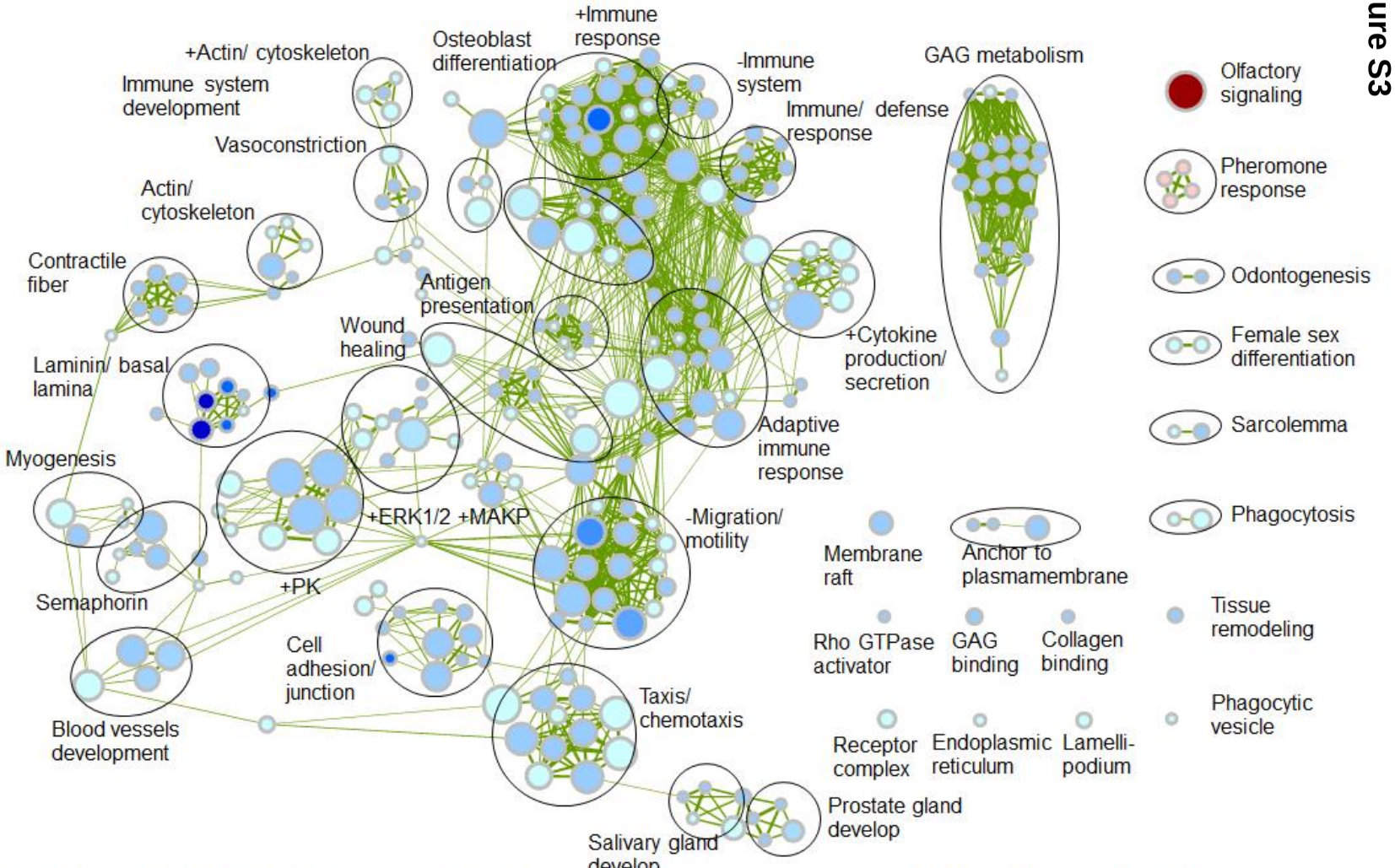
+Actin/ cytoskeleton
Immune system development
Osteoblast differentiation
+Immune response
-Immune system
Immune/ defense response
GAG metabolism
Olfactory signaling
Vasoconstriction
Actin/ cytoskeleton
Pheromone response
Contractile fiber
Antigen presentation
Odontogenesis
Wound healing
Female sex differentiation
Laminin/ basal lamina
+Cytokine production/ secretion
Sarcolemma
Adaptive immune response
Myogenesis
+ERK1/2 +MAKP
-Migration/ motility
Phagocytosis
Membrane raft
Anchor to plasmamembrane
+PK
Semaphorin
Tissue remodeling
Rho GTPase activator
GAG binding
Collagen binding
Cell adhesion/ junction
Taxis/ chemotaxis
Phagocytic vesicle
Blood vessels development
Receptor complex
Endoplasmic reticulum
Lamelli-podium
Prostate gland develop
Salivary gland develop
P value < 0.001; FDR Q Value < 0.001
Node size proportional to gene-set size
Jaccard Overlap Combined Cut-off: 0.275
Test used: Jaccard Overlap Combined Index (k constant = 0.5)
Node colour intensity proportional to enrichment score
-3
0
+3.8
75%
90%
95%
100%

Figure S4

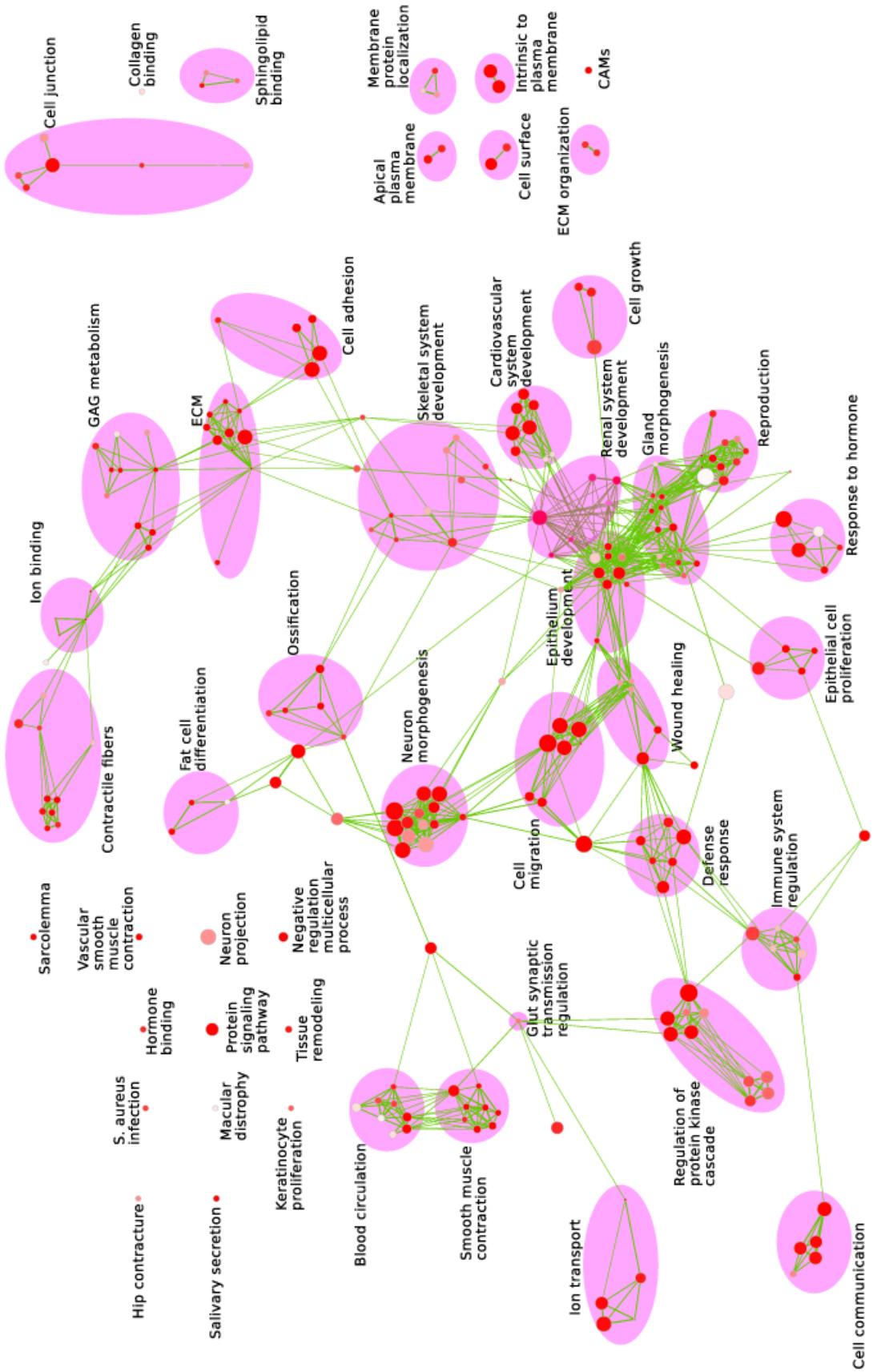
Cell junction
Collagen binding
Sphingolipid binding
Membrane protein localization
Intrinsic to plasma membrane
CAMs
Apical plasma membrane
Cell surface
ECM organization
GAG metabolism
ECM
Cell adhesion
Skeletal system development
Cardiovascular system development
Cell growth
Renal system development
Gland morphogenesis
Reproduction
Response to hormone
Ion binding
Contractile fibers
Ossification
Fat cell differentiation
Neuron morphogenesis
Epithelium development
Wound healing
Epithelial cell proliferation
Sarcolemma
Vascular smooth muscle contraction
Neuron projection
Negative regulation multicellular process
Cell migration
Defense response
Immune system regulation
Hormone binding
Protein signaling pathway
Tissue remodeling
Glut synaptic transmission regulation
S. aureus infection
Macular distrophy
Keratinocyte proliferation
Regulation of protein kinase cascade
Hip contracture
Salivary secretion
Blood circulation
Smooth muscle contraction
Ion transport
Cell communication
P value < 0.05

Figure S5

Region	Event	Freq. in PDA (%)	Freq. in AME (%)	Gene Symbols
chr4:140,989,635-140,992,922	CN Loss	80	0	Gm694
chr6:125,678,520-125,697,798	CN Gain	80	0	Ano2
chr6:130,334,179-130,413,964	CN Gain	80	0	Klra1
chr6:137,128,694-137,132,525	CN Gain	80	0	
chr6:137,792,844-137,807,440	CN Gain	80	0	
chr12:79,949,645-79,962,242	CN Gain	0	80	Atp6v1d
chr12:114,659,196-114,668,491	CN Loss	0	80	Igh-A (1g2), Gm16844, Igh, Ighg, V00821, abParts
chr12:114,668,491-114,676,477	CN Loss	0	100	abParts
chr12:114,715,396-114,722,266	CN Gain	0	80	abParts
chr12:117,668,003-117,679,572	CN Gain	20	100	Ncapg2
chr13:36,129,995-36,140,576	CN Loss	80	0	Lyrm4
chr14:51,574,375-51,586,687	CN Gain	80	0	Pnp2
chr14:52,494,308-52,502,775	CN Gain	80	0	
chr14:52,575,120-52,593,014	CN Gain	80	0	
chr19:17,165,722-17,173,735	CN Loss	80	0	Prune2

Figure S6

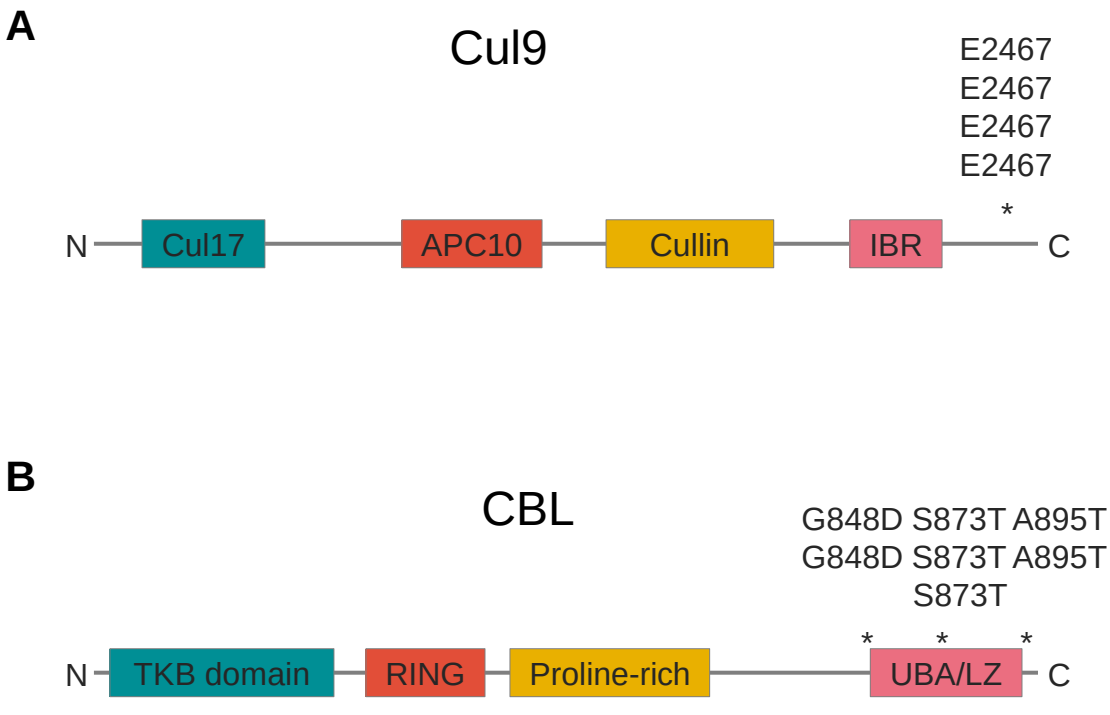
A
Cul9
E2467
E2467
E2467
E2467
*
N
Cul17
APC10
Cullin
IBR
C
B
CBL
G848D S873T A895T
G848D S873T A895T
S873T
* * *
N
TKB domain
RING
Proline-rich
UBA/LZ
C

Figure S7

A

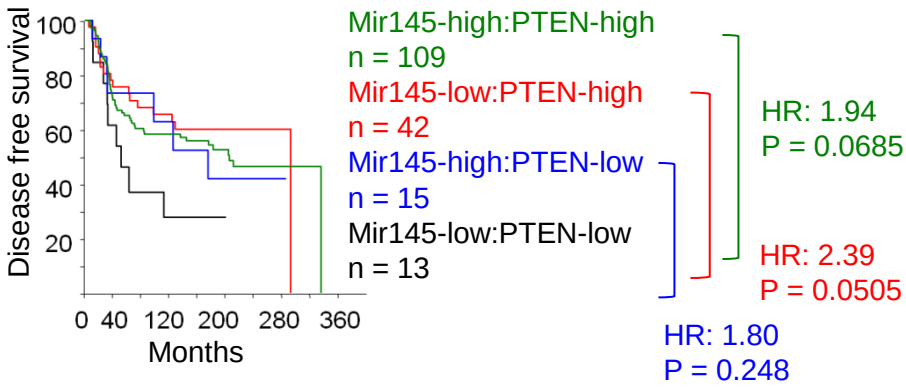
Disease free survival
100
80
60
40
20
0 40 120 200 280 360
Months
Mir145-high:PTEN-high
n = 109
Mir145-low:PTEN-high
n = 42
Mir145-high:PTEN-low
n = 15
Mir145-low:PTEN-low
n = 13
HR: 1.94
P = 0.0685
HR: 2.39
P = 0.0505
HR: 1.80
P = 0.248

Figure S8

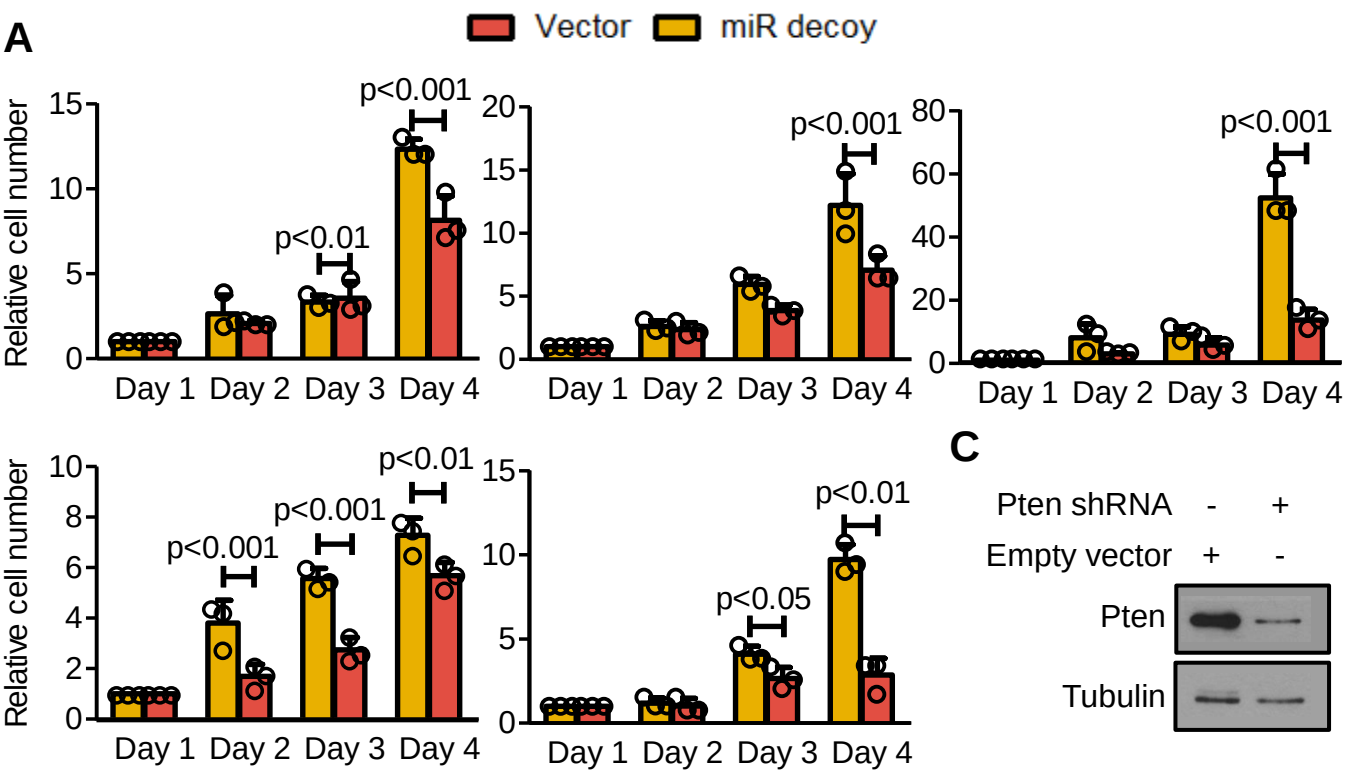

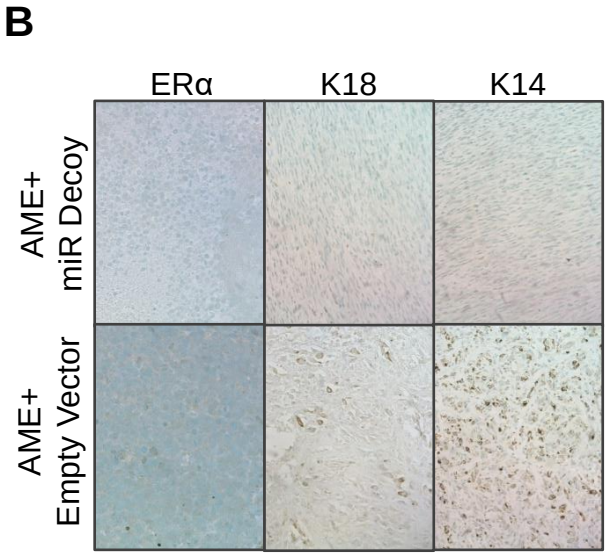

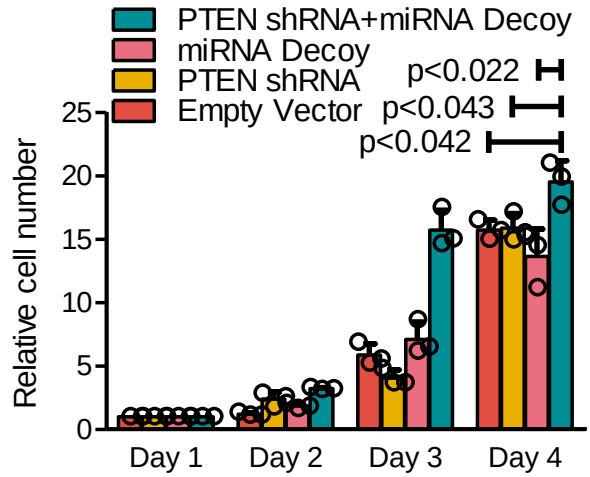

E

Double infection vs. Pten shRNA	Double infection vs. miR Decoy
2.738028	2.796179
1.879799	1.688193
2.566781	1.558011
2.408793	1.790536
1.402015	1.578207
2.518604	2.348223
5.382340739	2.221455044
5.952524144	3.668324576

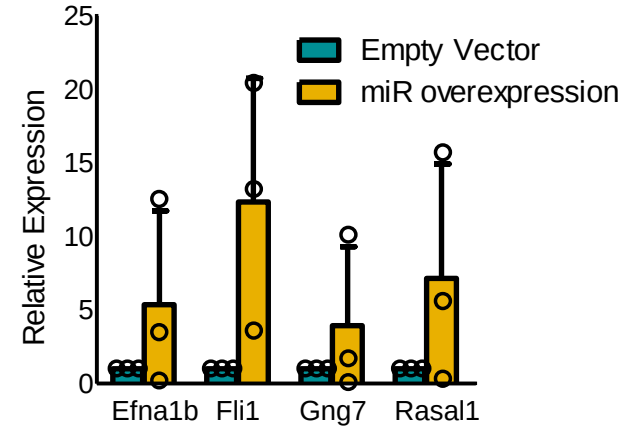

Figure S9

Pathway	AMEs	PDAs	p value
AKT	0.48041	0.386916	0.120221
β-catenin	0.275591	0.577568	0.092178
E2F1	0.297701	0.396888	0.255529
EGFR	0.456918	0.396238	0.356287
ER*	0.04189	0.775224	7.49E-05
Her2	0.394228	0.448001	0.581988
IFNα*	0.499751	0.279422	0.001646
IFN gamma	0.317352	0.283905	0.547193
Myc	0.28791	0.454292	0.177517
p53	0.520215	0.505344	0.806167
p63	0.692959	0.575521	0.379592
PI3K	0.600866	0.61257	0.886442
PR	0.273898	0.122126	0.081602
Ras*	0.468508	0.713203	0.001794
Src	0.663806	0.504662	0.266863
STAT3	0.576253	0.519356	0.241694
TGFβ*	0.331704	0.63198	0.005339
TNFα*	0.309567	0.194076	0.001017